Electronic Supplementary Material (ESI) for Journal of Materials Chemistry A.

Supplementary Information

Zn Nanosheet Coated with ZnS Subnanometer Layer for Effective and Durable CO_2 Reduction

Cheng-Long Li, Gu-Rong Shen, Rui Zhang, De-Yao Wu, Cheng-Qin Zou, Hui Liu*, Cun-Ku Dong*, Xi-Wen Du*

Contents

1. Supplementary Methods

Chemicals. All the reagents were of analytical grade and used directly without further purification. Zn powder (99%), CS_2 (99.99%), Nafion solution (5%) were purchased from Aladdin Reagent. Zn foil (0.25 mm, 99.994%) and $KHCO_3$ (99.7%) was purchased from Alfa Aesar. Alcohol (99.9%), isopropyl alcohol (99.9%) and acetic acid (99.5%) were purchased from J&K Chemical.

Synthesis of S-Zn-S NSs. S-Zn-S NSs were synthesized via thermal evaporation in a two-temperature-zone tube furnace. Zn powder and FTO-coated glass were put in the high and low temperature zones, respectively. Before the synthesis, the tube was exhausted to vacuum and then filled with N_2 and CS_2 gas with flow rates of 8 and 2 sccm, respectively. Zn powder and FTO were heated up to 420 and 200 ℃, respectively, and the temperatures were kept for an hour. The pressure in the tube was maintained at 1.6 Torr during the reaction process. Afterwards, the furnace was cooled down naturally to room temperature. As such, S-Zn-S NSs grew up as arrays on the FTO substrate.

Synthesis of Zn@ZnS NSs. To prepare Zn@ZnS NSs, the FTO substrate was heated to 300 ℃, and the other synthetic parameters are the same as those for the synthesis of S-Zn-S NSs.

Synthesis of pure Zn NSs. The as-prepared S-Zn-S NSs were reduced by constant potential electrolysis at -1.3 V vs. RHE for 30 min in N_2-saturated 0.1 M $KHCO_3$ solution.

Synthesis of ZnS PML. The as-synthesized S-Zn-S NSs was etched in 10% diluted acetic acid to remove the Zn by the following reaction：$2CH_3COOH + Zn = (CH_3COO)_2Zn + H_2$

The etching treatment was kept for 48 hours, finally, pure ZnS PML was obtained by centrifuging the solution.

2. Material Characterization

The morphology of samples were observed in HITACHI S-4800 scanning electron microscope (SEM) operated at 5.0 kV. Transmission electron microscopy (TEM), high-resolution TEM images (HRTEM), energy dispersive spectrometer (EDS), EDS mapping and electron energy loss spectroscopy (EELS) were taken in FEI Tecnai G2 F20 transmission electron microscope operated at 200 kV. X-ray diffraction (XRD) measurements were carried out on Bruker D8 X-ray diffraction diffractometer with Cu Ka radiation. X-ray photoelectron spectroscopy (XPS) analysis was performed using a PHI Quantum 2000 scanning ESCA Microprobe spectrometer. Atomic force microscopy (AFM) measurement was done with a Vecco IIIa Nanoscope in the tapping mode, and the sample was prepared onto a silicon substrate by drop-drying the aqueous solution of the sample.

3. Electrochemical characterization

Electrode Preparation. The catalyst ink was prepared by dispersing 1 mg of catalyst powder in 400 μL mixture of isopropyl alcohol and ultrapure water (1:1, v/v), and then added 20 μL of Nafion solution (5 wt%) followed by ultrasonication for 5 min. Then 7 μL of the ink was loaded onto a glassy carbon electrode, with a diameter of 5 mm, which was used as the working electrode.

Electrochemical Tests. All electrochemical CO_2 reduction experiments were performed using a three-electrode system connected to an electrochemical workstation (CHI, 600E). The measurement system was composed of a working electrode (catalyst was loaded on glassy carbon electrode), a counter electrode (graphite) and a reference electrode (saturated calomel electrode, SCE). The applied potentials were converted with respect to reversible hydrogen electrode (RHE), E(RHE) = E(SCE) + 0.0591 pH + 0.242 V.

The experiments were carried out in a gas-tight two-compartment H-cell separated by Nafion membrane. The electrolyte was CO_2-saturated 0.1 M $KHCO_3$ aqueous solution (pH=6.8) and be

stirred at a rate of 500 rpm during all the testing process. CO_2 gas (99.99%) flowed with a rate of 20 sccm controlled by a mass flow controller (MFC, MKS Instruments Inc.) into electrolyte for an hour to get saturated before testing. During electrolysis, CO_2 gas was delivered into the cathodic compartment and was routed into a gas chromatograph (Agilent, 7890B). Online electrochemical gas chromatograph was employed to detect gas products and estimate their Faradaic efficiencies.

The gas products from the cathode compartment were analyzed using an Agilent 7890B gas chromatograph (GC) equipped with five Capillary columns (Agilent J&W GC column), two thermal conductivity detectors (TCD1, TCD2) and a flame ionization detector (FID). Gaseous products are separated in the capillary column, and a thermal conductivity detector (TCD1) is used to quantify CO, a thermal conductivity detector (TCD2) is used to quantify H_2, a flame ionization detectors (FID) is used to quantify hydrocarbon. He (99.999%) and N_2 (99.999%) were used as the carrier gases, and standard gas (H_2, C_2H_4, C_3H_8, CO, C_2H_6, CO_2, CH_4, C_3H_6) were used to make calibration.

The linear scan voltammogram (LSV) was measured ranging from -0.55 to -1.2 V (vs.RHE) at a scan rate of 50 mV s^{-1}. For the calculation of Faradaic efficiency (FE), the instantaneous current was measured at a constant potential, and each potential was tested for at least 2 hours. The data were calculated by the following equation.

$$FE(\%) = \frac{nZF}{Q} \times 100\% = \frac{m_0 \cdot \frac{A}{A_0} \cdot vZF}{M \cdot i} \times 100\%$$

Where n is the amount of substance, Z is the electron transfer number (CO and H_2 is 2), F is the Faraday's constant (96,485 C mol^{-1}), m_0 is the amount of standard gas, A is the peak area of detection, A_0 is the peak area of standard gas, v is the gas flow rate (20 sccm), M is the relative molecular mass, i is the instantaneous current.

The electrochemical surface area (ECSA) was calculated by the following equation: ECSA= $R_f \cdot S$, R_f is the roughness factor of the catalysts estimated by measuring an electric double layer capacitance (C_{dl}), and the C_{dl} of the as-prepared catalysts was derived from the Cyclic voltammetry (CV) curves at different scan rate (5, 10, 15, 20, 25, 30 $mV.s^{-1}$) in the N_2-bubbled 0.1 M $KHCO_3$ electrolyte. *S* is the surface area of the glassy carbon electrode (0.196 cm^2).

TOF for CO was calculated by the following equation.

$$TOF_{CO}(h^{-1}) = \frac{Turnover\ number\ of\ CO\ formation\ /\ geometric\ \ area}{active\ sites\ density} = \frac{j_{CO} \cdot 3600}{2 \cdot N \cdot F}$$

Here, *N* is the number of active sites per cm^2, *F* is the Faraday's constant, j_{CO} is the CO current density at different applied potential.

Tafel slopes were obtained by plotting overpotential (η) against *log* (j_{CO}) and using the following equation.

$$\eta(V) = E - 0.11(V)$$

$$j_{CO}(mA \cdot cm^{-2}) = FE \cdot I(mA \cdot cm^{-2})$$

Here, *E* is the apply potential (vs. RHE), *I* is the corresponding geometrical current density.

EIS was measured at a potential of -0.8V (vs. RHE) and in a frequency range from 10^{-1} to 10^6 Hz

4. DFT calculations

The calculations were performed with the VASP package[1-2], using Perdew–Burke–Ernzerhof (PBE)[3] of exchange correlation energy functional based on a generalized gradient approximation and the projector augmented wave (PAW)[4] method. Kohn-Sham wave functions of the valence electrons were expanded in a plane wave basis with an energy cut-off value of 500 eV. Brillouin zone sampling was conducted using a Monkhorst Pack grid of 5 × 5 × 1 k-points. The dipole correction was applied along the z-direction, the 4×4 model surface slabs were constructed with three layers

(bottom one layer fixed), with vacuum layers of at least 15 Å. Ionic relaxation was converged until forces were reduced to within 0.03 eV/Angstrom for the non-constrained atoms.

2. Supplementary Figures

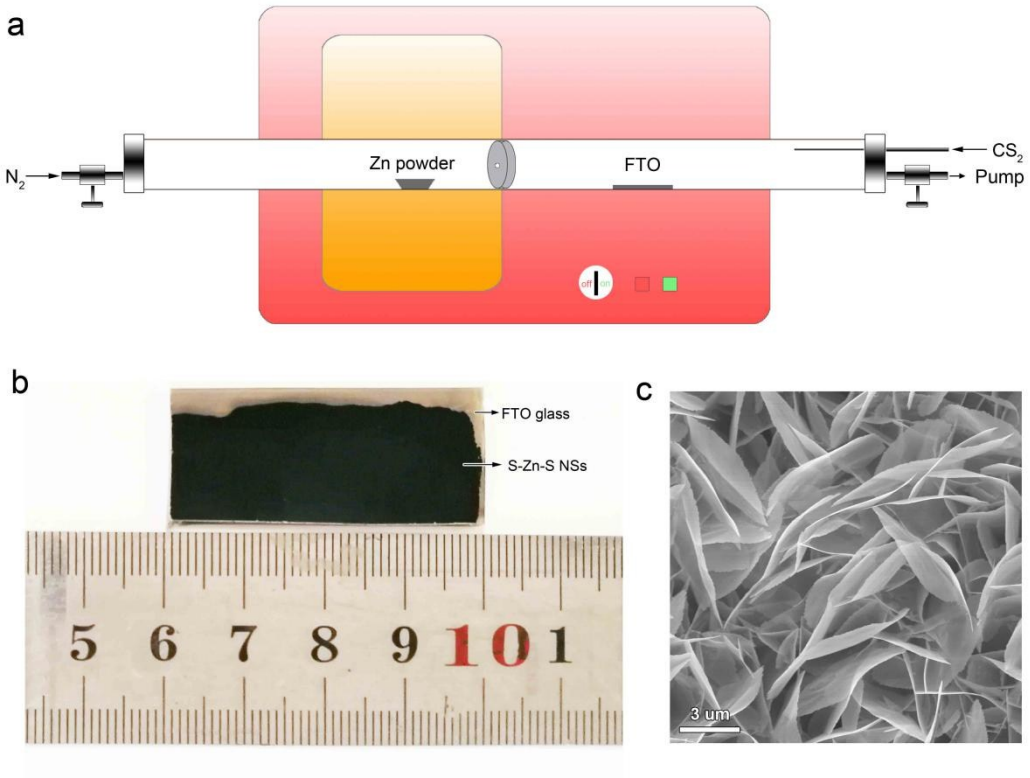

Figure S1. (a) Experimental setup illustrating the thermal evaporation process in a two-temperature tube furnace. (b) Photograph of S-Zn-S NSs on a piece of 1.5 cm×4 cm FTO glass. (c) SEM images of S-Zn-S NSs.

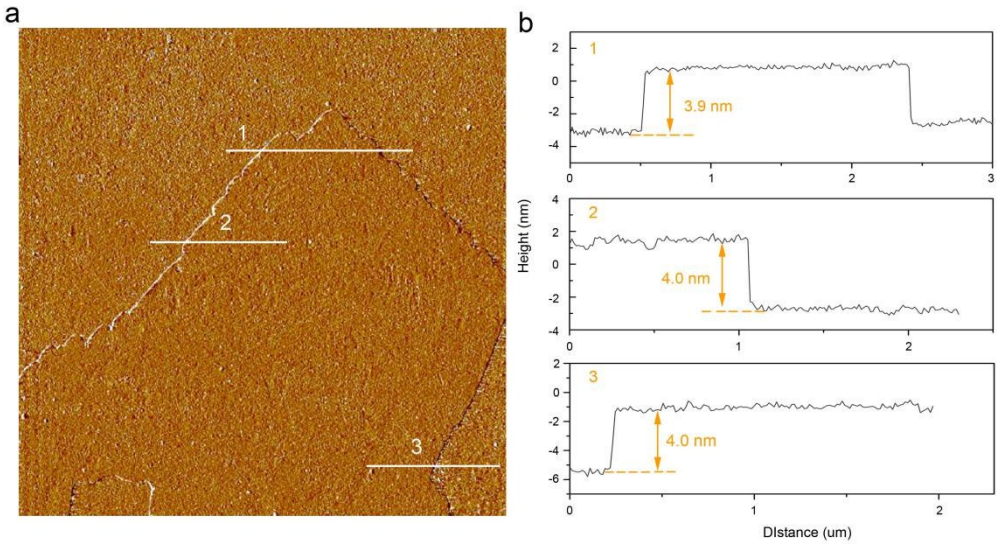

Figure S2. (a) AFM image of S-Zn-S NSs on a silicon substrate. (b) the corresponding profile.

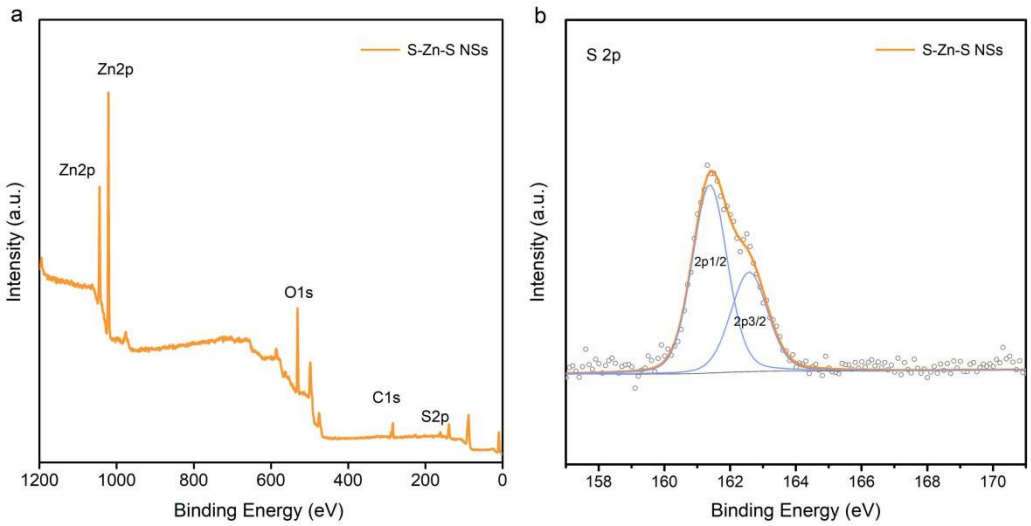

Figure S3. (a) XPS survey spectrum of S-Zn-S NSs. (b) S 2p of S-Zn-S NSs. The atomic ratio of elements is summarized in Table S1.

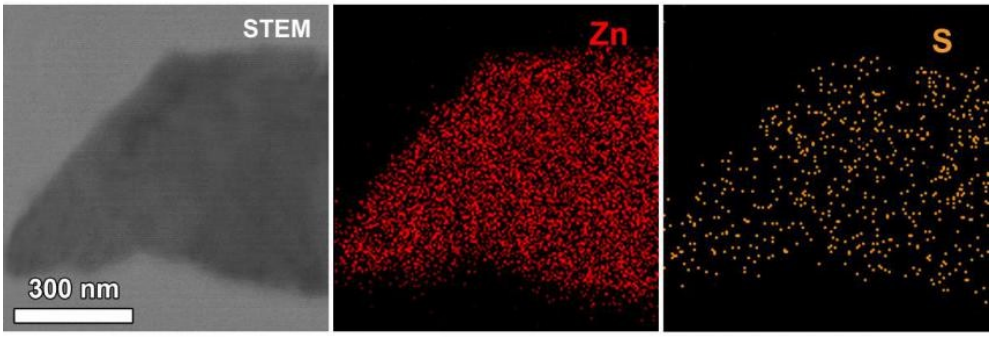

Figure S4. EDS mapping of S-Zn-S NSs.

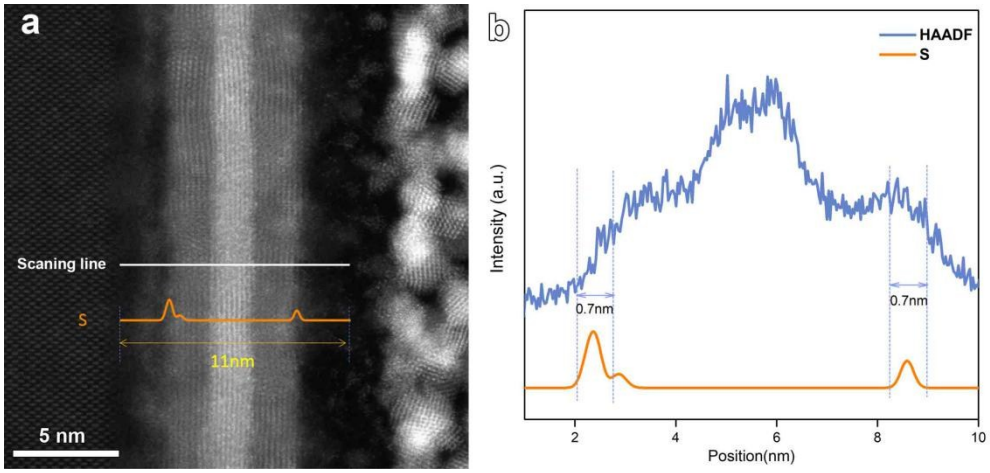

Figure S5. (a)The side-view HRTEM image of S-Zn-S NSs. (b) Line scan profile of S-Zn-S NSs.

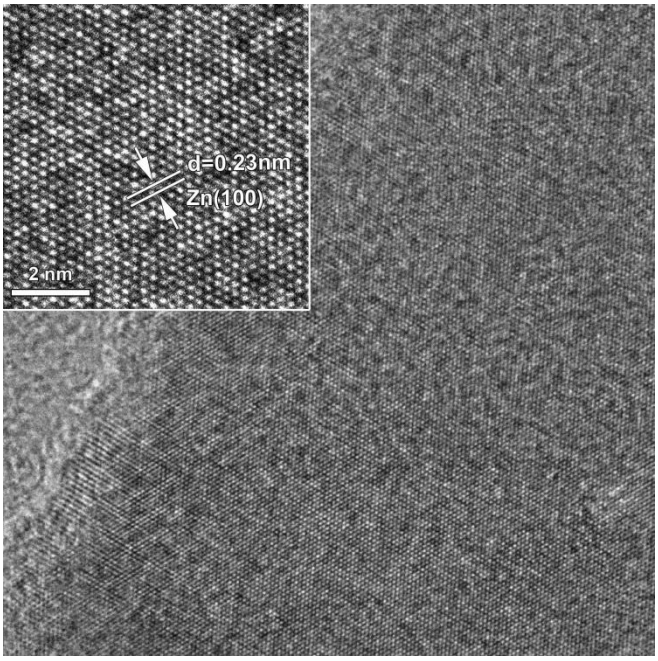

Figure S6. HRTEM image of S-Zn-S NSs.

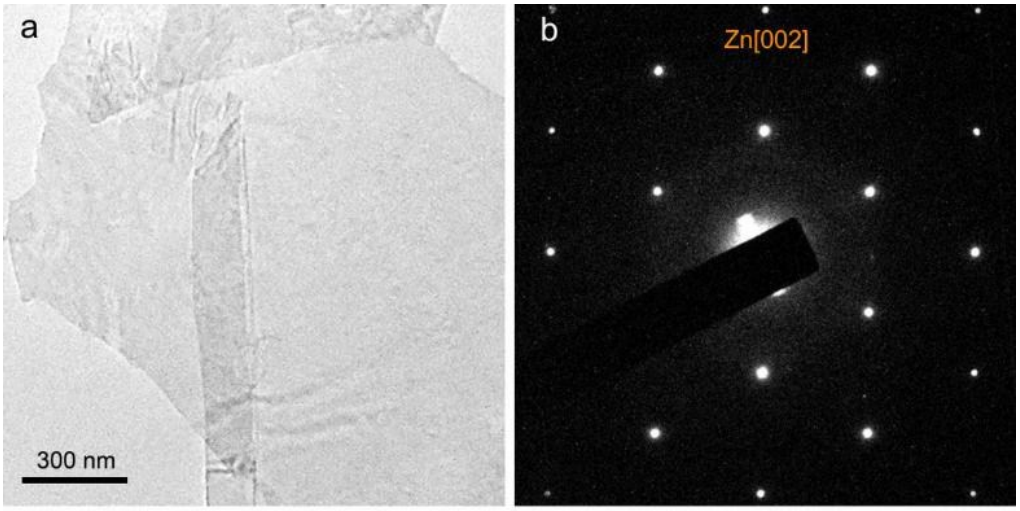

Figure S7. (a) TEM image of S-Zn-S NSs. (b) SAED pattern of S-Zn-S NSs.

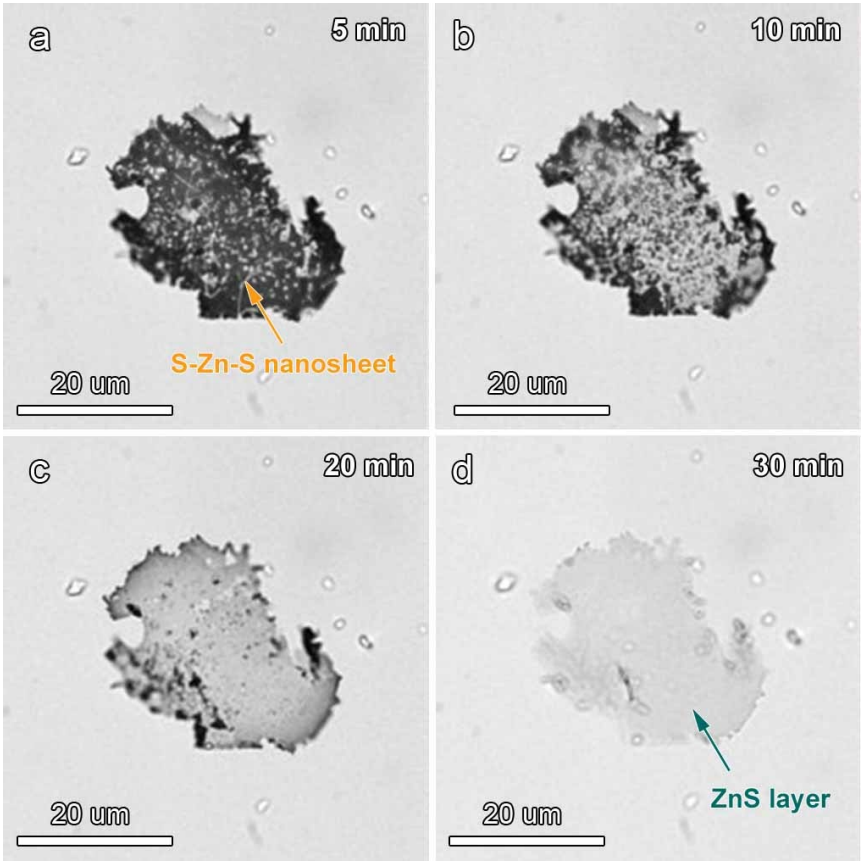

Figure S8. The optical microscopy images of S-Zn-S NSs after different etching time. (a) 5 min. (b) 10 min (c) 20 min (d) 30 min.

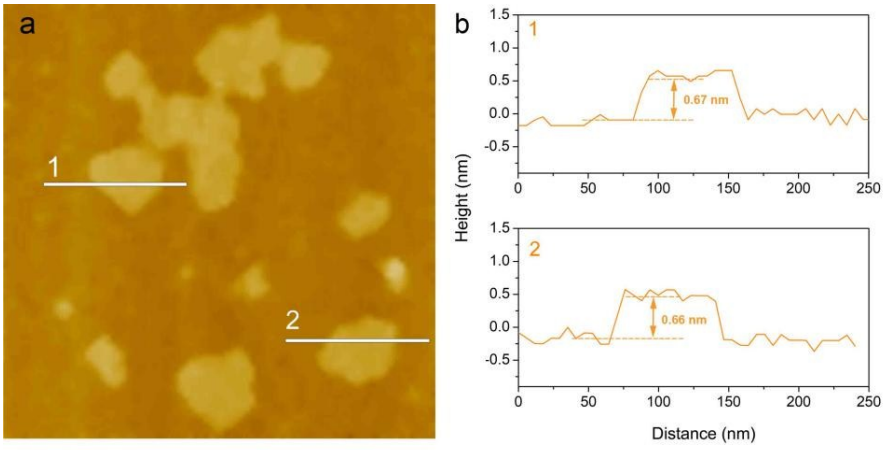

Figure S9. (a)The AFM image of the ZnS subnanometer layer by etching S-Zn-S NSs. (b) the corresponding height profile.

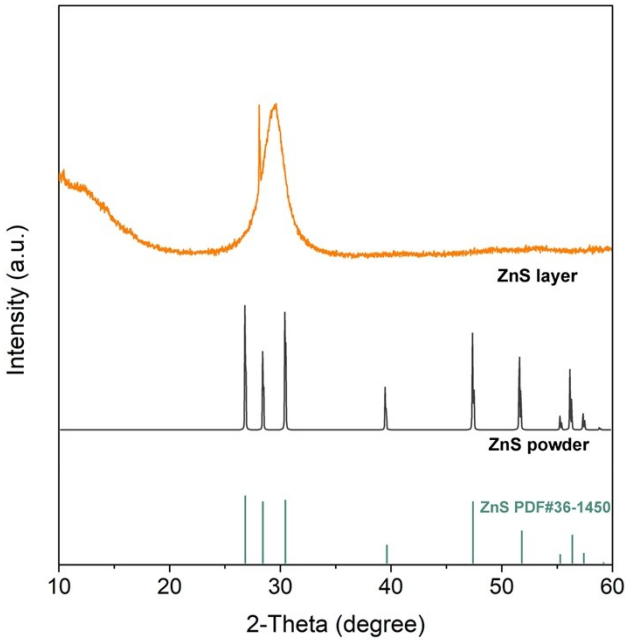

Figure S10. XRD pattern of ZnS subnanometer layer.

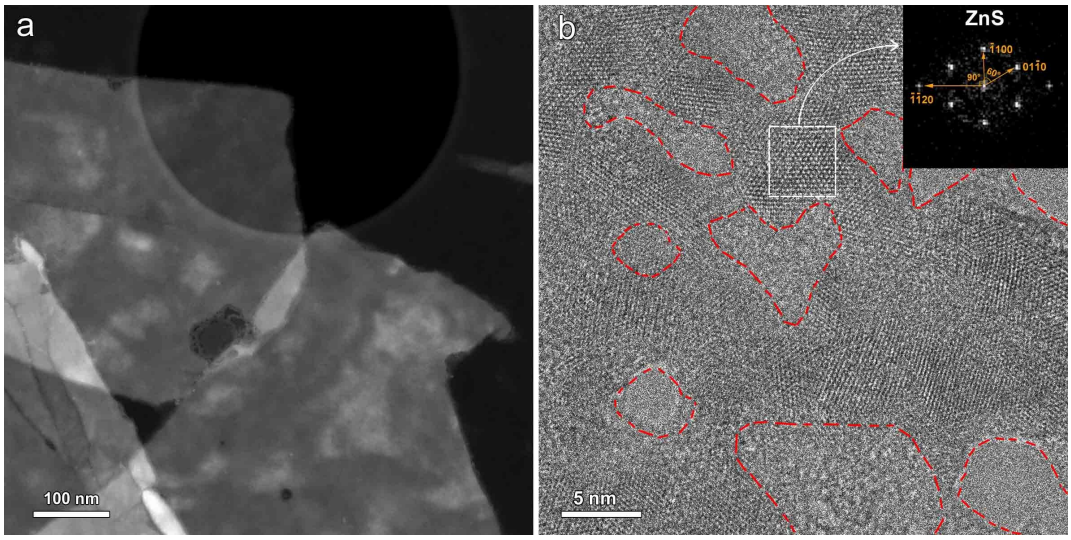

Figure S11. In-suit heating of S-Zn-S NSs in TEM. (a) TEM image of S-Zn-S NSs before heating. (b) HRTEM image of porous ZnS subnanometer layer, inset shows the FFT image.

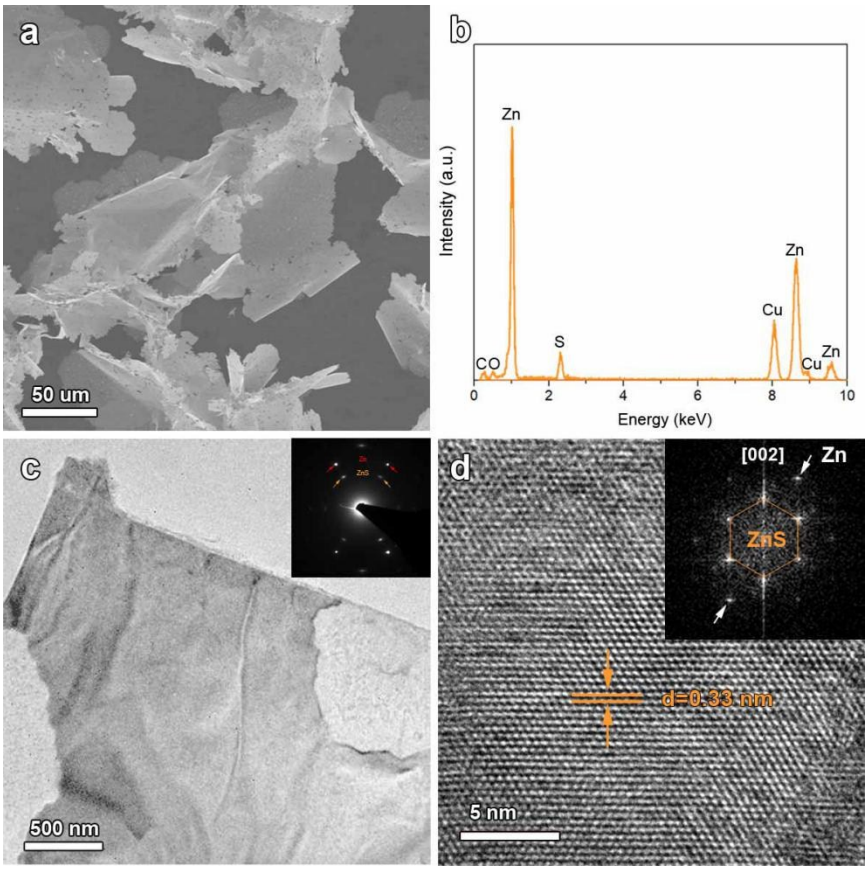

Fig S12. Characterizations of Zn@ZnS NSs (a) SEM image (b) EDS spectrum, the atomic ratio of elements is summarized in Table S1. (c) TEM image, inset is SAED pattern. (d) HRTEM image of Zn@ZnS NSs, inset is the fast Fourier transform pattern.

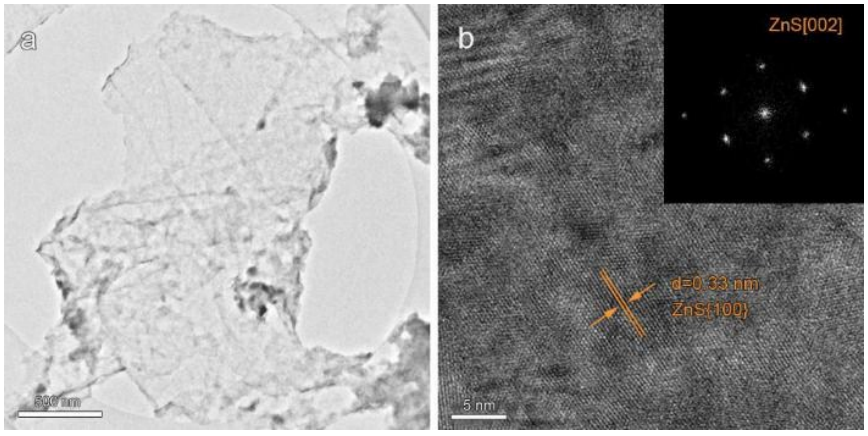

Figure S13. Characterizations of ZnS layer obtained by etching Zn@ZnS NSs (a) TEM image. (b) HRTEM image, inset is the FFT pattern.

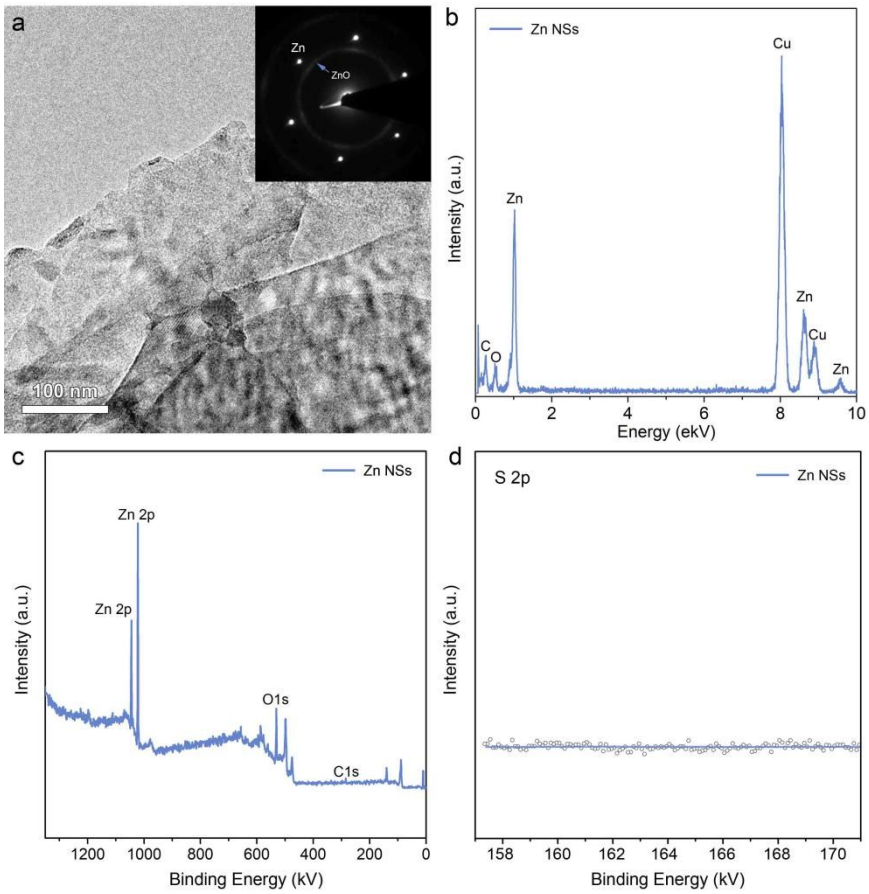

Fig S14. Characterizations of Zn NSs. (a) TEM image, inset is SAED pattern. (b) EDS spectrum of. (c) XPS survey spectrum. (d) S 2p XPS spectrum. The atomic ratio of elements is summarized in Table S1.

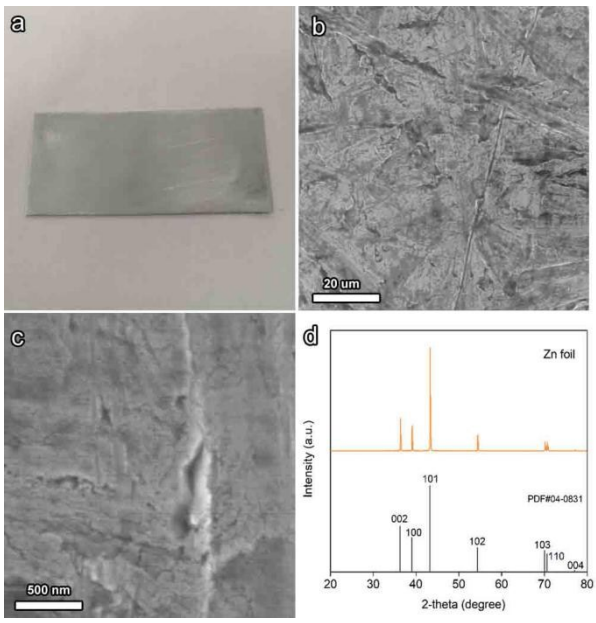

Fig S15. Characterizations of Zn foil. (a) optical image, (b) low magnification SEM image, (c) high magnification SEM image, (d) XRD pattern.

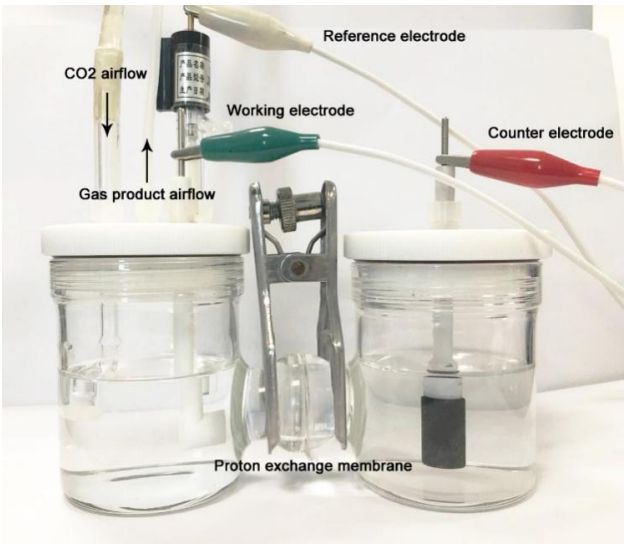

Figure S16. The three-electrode gas tight two-compartment system. A L-type glassy carbon electrode with a diameter of 5 mm was used as the working electrode, a saturated calomel electrode (SCE) as the reference electrode, and graphite as the counter electrode. The electrolyte was CO_2-saturated 0.1 M $KHCO_3$ aqueous solutions (pH=6.8) and stirred by the magnet at a rate of 500 rpm during all the testing process. A 20 sccm flow of CO_2 gas was introduced into the electrolyte and maintained during the whole testing process. Product airflow was routed into a gas chromatograph (GC).

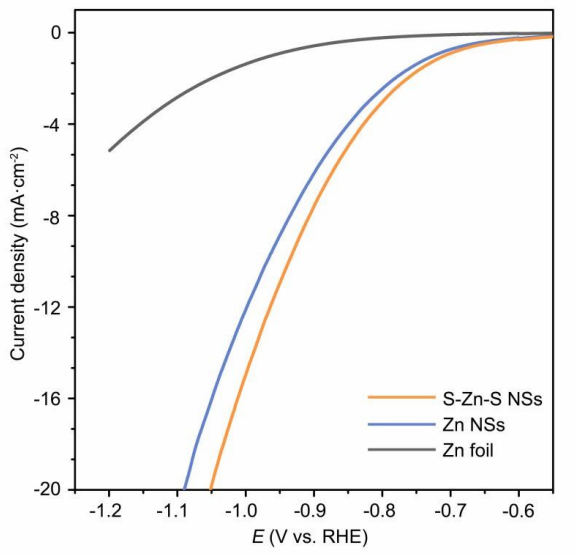

Figure S17. LSV curves of S-Zn-S NSs, Zn NSs and Zn foil in CO_2-saturated 0.1 M $KHCO_3$ (pH 6.8) electrolyte.

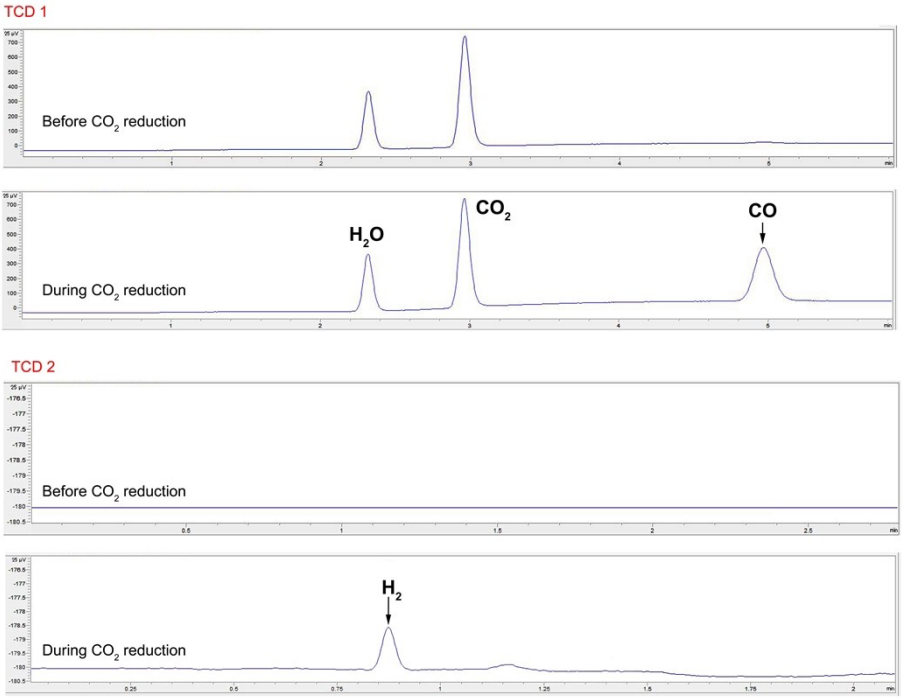

Figure S18. Gas chromatography (GC) spectra before and during CO_2 reduction. The retention times of CO and H_2 were about 4.9 and 0.9 min, respectively.

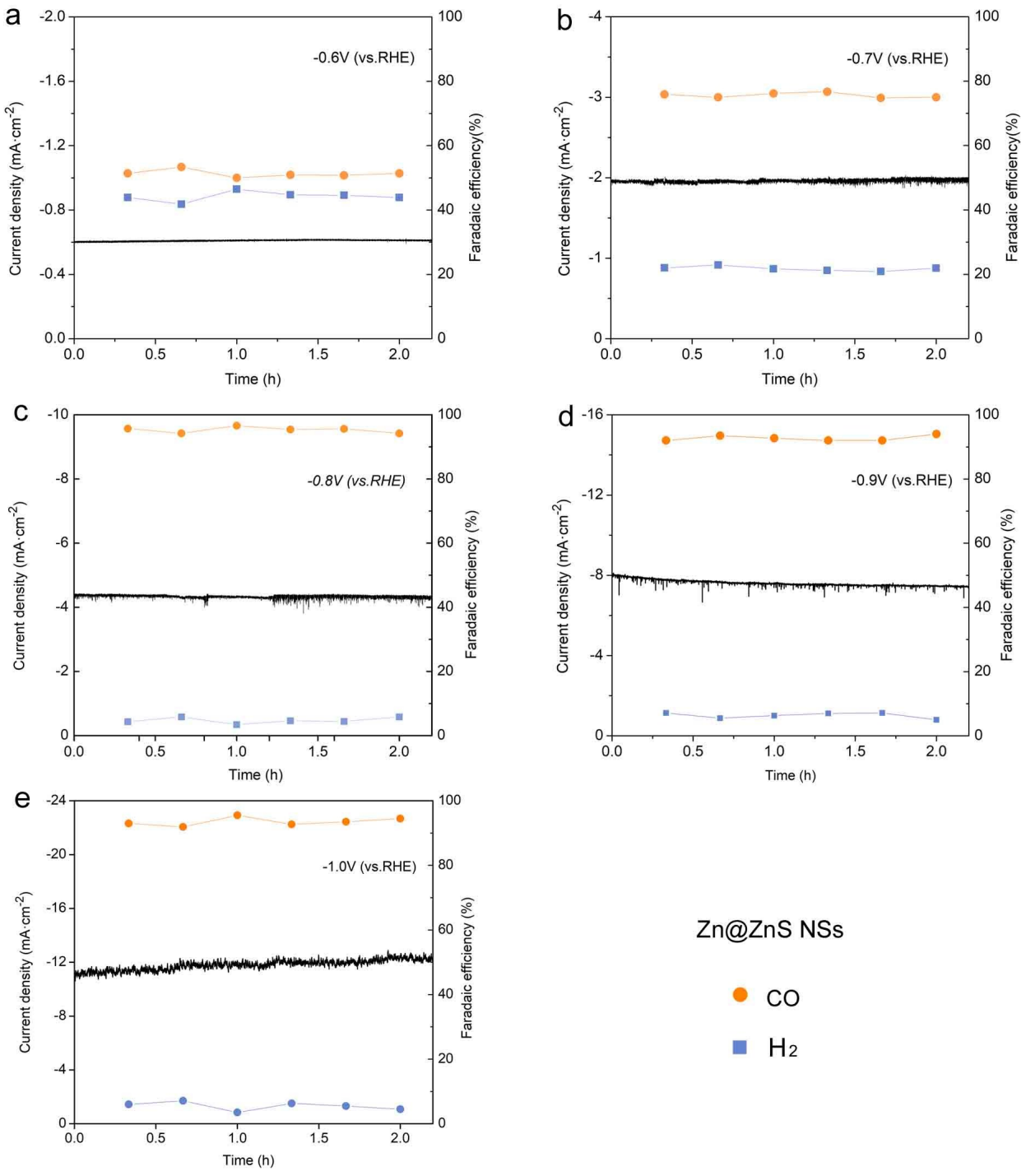

Figure S19. The total current density (left axis) and the gas faradaic efficiency (right axis) of S-Zn-S NSs at different potentials (a) -0.6 V, (b) -0.7 V, (c) -0.8 V, (d) -0.9V, (e) -1.0 V (vs. RHE) in CO_2-saturated 0.1M $KHCO_3$ electrolyte.

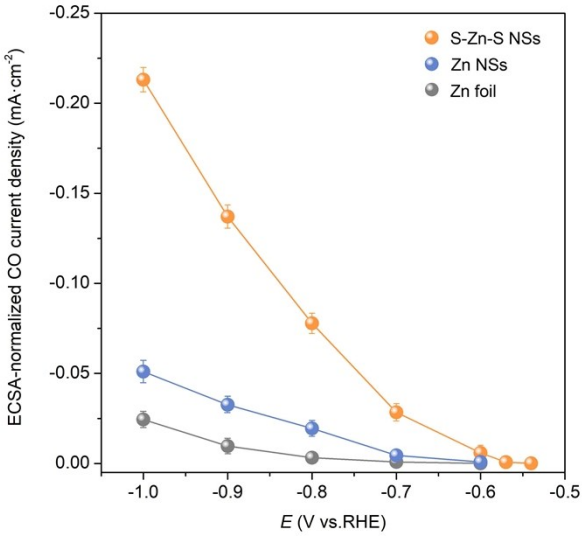

Figure S20. ECSA-normalized CO current densities of S-Zn-S NSs, Zn NSs and Zn foil at different applied potentials.

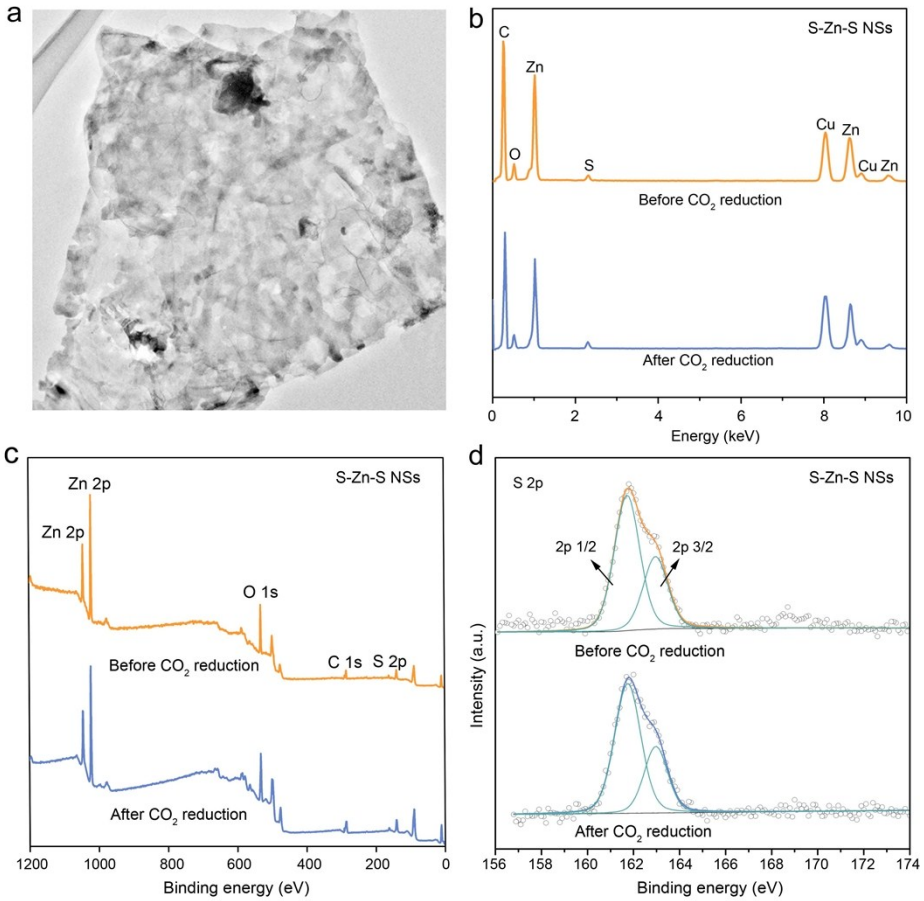

Figure S21. Characterizations of S-Zn-S NSs after CO_2 reduction. (a) TEM image. (b) EDS spectrum, the atomic ratio of elements is summarized in Table S1. (c) XPS survey spectrum. (d) S 2p XPS spectrum.

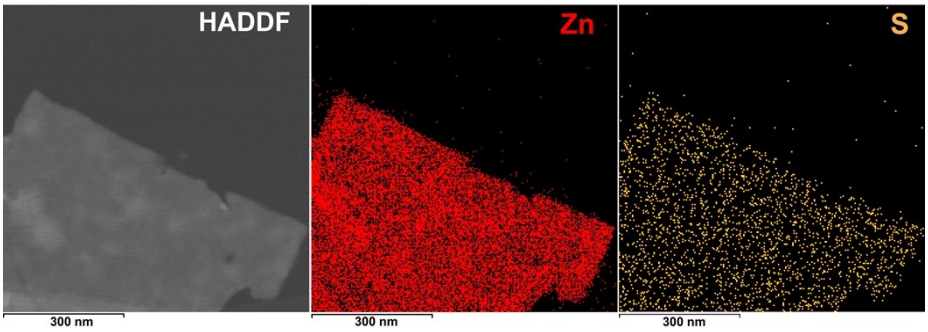

Figure S22. EDS mapping of S-Zn-S NSs after CO_2 reduction.

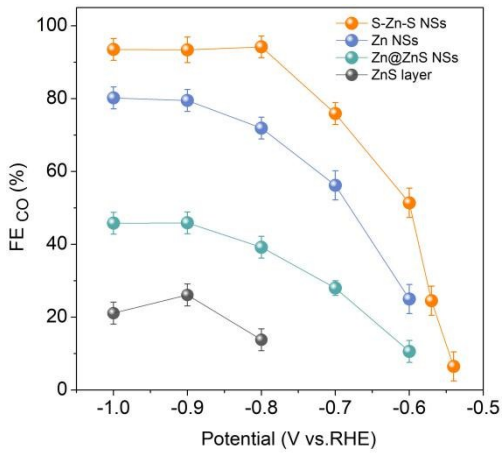

Figure S23. Faradaic efficiencies of CO for S-Zn-S NSs, Zn NSs, Zn@ZnS NSs and ZnS layer at different applied potentials.

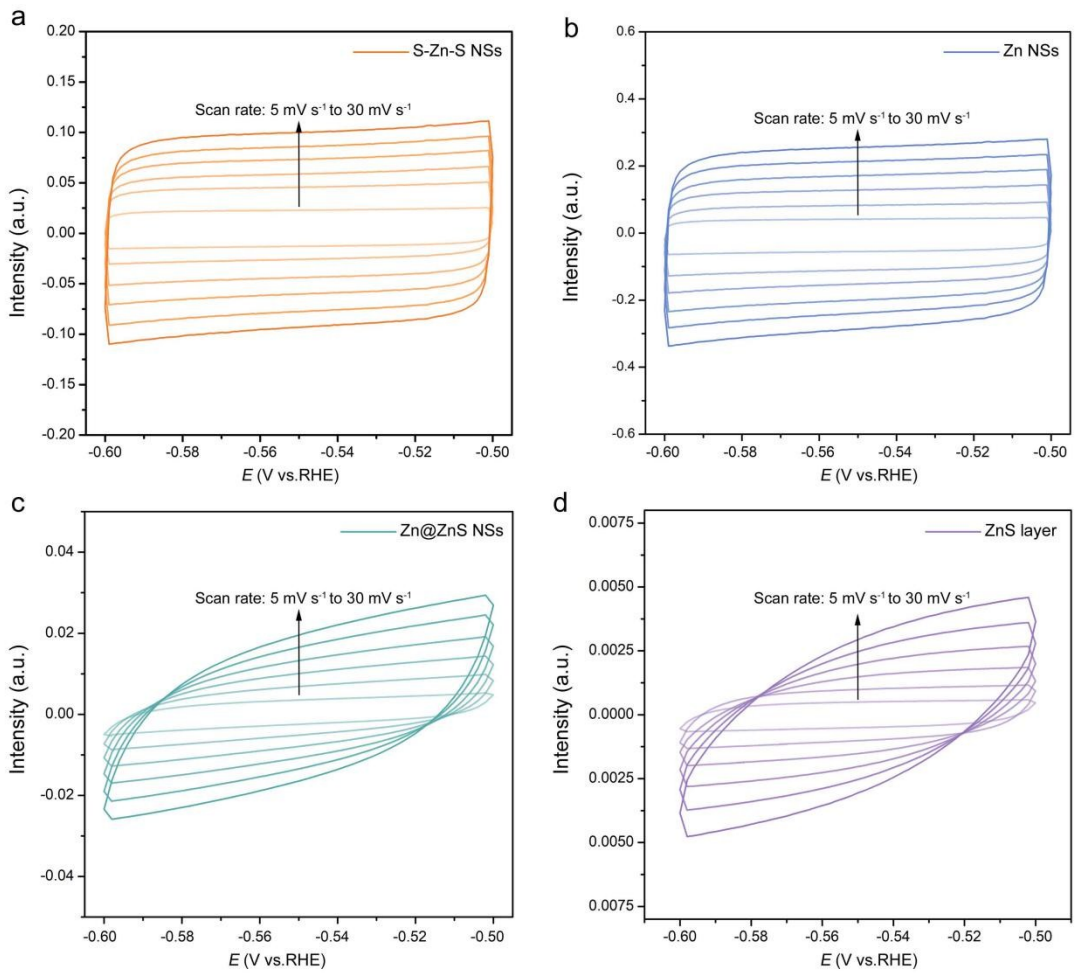

Figure S24. Cyclic voltammograms curves at various scan rates (5, 10, 15, 20, 25 and 30 mVs^{-1}). (**a**) S-Zn-S NSs (**b**) Zn NSs (**c**) Zn@ZnS NSs (d) ZnS layer.

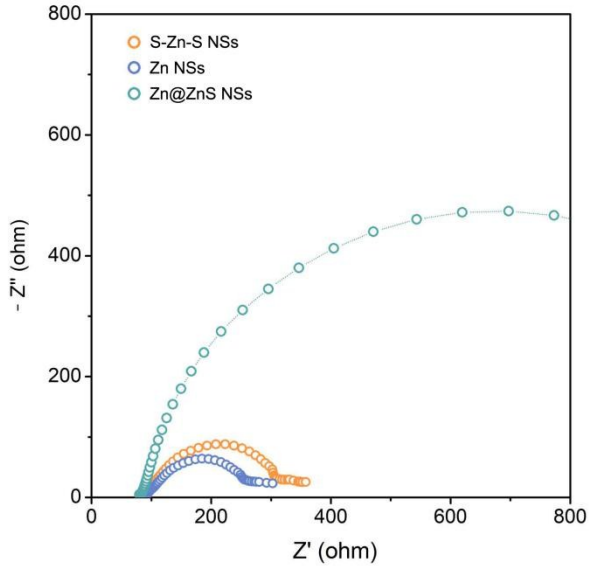

Figure S25. Electrochemical impedance spectra of S-Zn-S NSs, Zn NSs, and Zn@ZnS NSs.

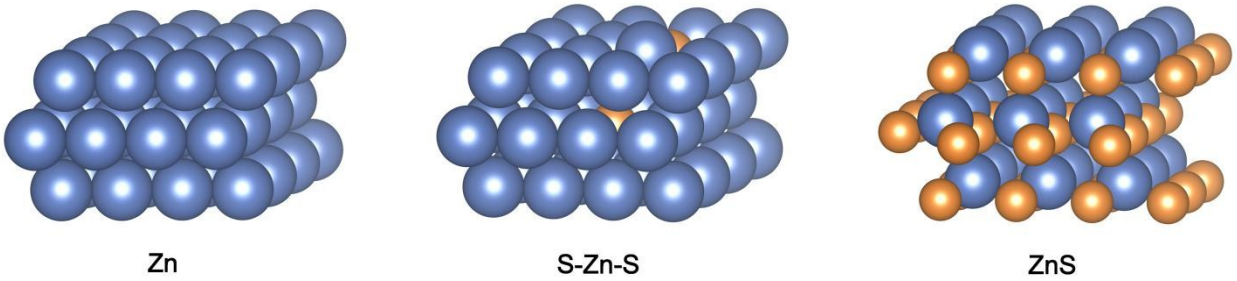

Figure S26 Structural models of Zn, S-Zn-S, and ZnS for DFT calculation.

3. Supplementary Tables

Table S1. Elemental ratio of S for as-prepared samples.

Samples	EDS	XPS
S-Zn-S NSs	6.72 %	7.10%
S-Zn-S NSs after test	6.38 %	6.80 %
Zn@ZnS NSs	13.18 %	13.07 %
Zn NSs	0	0

Table S2. Summary of CO_2RR performance of S-Zn-S NSs in CO_2-saturated 0.1 M $KHCO_3$ electrolyte.

Potential (V vs. RHE)	iR-correct (V vs. RHE)	Curent density (mA cm^{-2})	FE_{CO} (%)	FE_{H2} (%)	J_{CO} (mA cm^{-2})	J_{H2} (mA cm^{-2})
-0.54	-0.539	-0.06	6.5	92.5	-0.0039	-0.056
-0.57	-0.568	-0.10	24.5	74.1	-0.025	-0.074
-0.60	-0.595	-0.60	51.4	47.9	-0.31	-0.29
-0.70	-0.668	-1.93	75.9	23.0	-1.46	-0.44
-0.80	-0.729	-4.28	94.2	5.6	-4.03	-0.24
-0.90	-0.773	-7.60	93.4	5.3	-7.10	-0.40
-1.00	-0.804	-11.75	93.5	6.1	-10.99	-0.72

Table S3. Summary of CO_2RR performance of Zn-based and other active metallic catalysts in bicarbonate electrolyte.

Samples	Electrolyte	Potential (vs. RHE)	Current density (mA cm^{-2})	FE (%)	Tafel slope (mV dec^{-1})	Reference
S-Zn-S NSs	0.1 M $KHCO_3$	-0.80	4.28	94.2	57	this work
V_O-rich ZnO	0.1 M $KHCO_3$	-1.10	16.1	83	72	[5]
Re-Zn	0.5 M $KHCO_3$	-0.90	6.6	77.8	—	[6]
LiET-Zn	0.1 M $KHCO_3$	-1.17	23	91.1	149	[7]
Hexagonal Zn	0.5 M $NaHCO_3$	-0.95	14.9	85.4	—	[8]
Zn Dendrites	0.5 M $KHCO_3$	-1.10	17	79	260	[9]
Nanoscale Zn	0.5 M $NaHCO_3$	-1.6 (vs.SCE)	—	57	—	[10]
CdS nanorods	0.1 M $KHCO_3$	-1.20	27.1	81	69	[11]
Fe-N-C	0.1M $KHCO_3$	-0.55	—	65	—	[12]
Ni-N-C	0.1M $KHCO_3$	0.78	—	85	—	
Cu@SnO_2	0.5 M $NaHCO_3$	-0.70	4.6	93	—	[13]
g-C_3N_4/MWCNTs	0.1M $KHCO_3$	-0.75	~-0.67	60	—	[14]
OD-Ag	0.1M $KHCO_3$	-0.80	1.15	89	77	[15]
Tri-Ag NPs	0.1M $KHCO_3$	-0.856	1.3	97	153	[16]
Au-CeO_2/C	0.1 M $KHCO_3$	-0.89	12.9	91	—	[17]

Table S4. The zero-point energy correction, and entropy correction for adsorbates on three different structures. All values are given in eV.

Structures	Adsorbates	ZPE	-TS
Zn	COOH*	0.60	-0.25
	CO*	0.17	-0.19
	H*	0.14	-0.05
ZnS	COOH*	0.62	-0.21
	CO*	0.17	-0.18
	H*	0.16	-0.02
S-Zn-S	COOH*	0.58	-0.28
	CO*	0.17	-0.19
	H*	0.14	-0.02

4. Supplementary References

1. G. Kresse, J. Furthmüller, Phys. Rev. B 1996, **54**, 11169.
2. G. Kresse, J. Furthmüller, Comp. Mater. Sci. 1996, **6**, 15-50.
3. J. P. Perdew, Burke, K. & Ernzerhof, Phys. Rev. Lett. 1997, **77**, 3865
4. G. Kresse, D. Joubert, Phys. Rev. B 1999, **59**, 1758.
5. Z. G. Geng, X. D. Kong, W. W. Chen, H. Y Su, Y. Liu, F. Cai, G. X. Wang, J. Zeng, Angew. Chem. Int. Ed. 2018, **57**, 1-7.
6. D. L. T. Nguyen, M. S. Jee, D. H. Won, H. Jung, H. S. Oh, B. K. Min, Y. J. Hwang, ACS Sustainable Chem. Eng. 2017, **5**, 11377-11386.
7. K. Jiang, H. Wang, W. B. Cai, H. T. Wang, ACS Nano 2017, **11**, 6451–6458.
8. D. H. Won, H. Shin, J. Koh, J. Chung, H. S. Lee, H. Kim, S. I. Woo, Angew. Chem. Int. Ed. 2016, **55**, 9297-9300.
9. J. Rosen, G. S. Hutchings, Q. Lu, R. V. Forest, A. Moore, F Jiao, ACS Catal. 2015, **5**, 4586-4591.
10. F. J. Quan, D. Zhong, H. C. Song, F. L. Jia, L. Z. Zhang, J. Mater. Chem. A 2015, **3**, 16409-16413.
11. R. He, A. Zhang, Y. L. Ding, T. Y. Kong, Q. Xiao, H. L. Li, Y. Liu, J. Zeng, Adv. Mater. 2018, **30**, 1705872.
12. W. Ju, A. Bagger, G. P. Hao, A. S. Varela, I. Sinev, V. Bon, B. R. Cuenya, S. Kaskel, J. Rossmeisl, P. Strasser, Nat. Commun. 2017, **8**, 944.
13. Q. Li, J. J. Fu, W. L. Zhu, Z. Z. Chen, B. Shen, L.H. Wu, Z. Xi, T. Y. Wang, G. Lu, J. J. Zhu, S. H. Sun, J. Am. Chem. Soc. 2017, **139**, 4290−4293.
14. X. Y. Lu, T. H. Tan, Y. H. Ng, R. Amal, Chem. Eur. J. 2016, **22**, 11991-11996.

15. M. Ma, B. J. Trzes´niewski, J. Xie, W. A. Smith, Angew. Chem. Int. Ed. 2016, **55**, 9748 - 9752.

16. S. B. Liu, H. B. Tao, L. Zeng, Q. Liu, Z. H. Xu, Q. X. Liu, J. L. Luo, J. Am. Chem. Soc. 2017, **139**, 2160-2163.

17. D. F. Gao, Y. Zhang, Z. W. Zhou, F. Cai, X. F. Zhao, W. G. Huang, Y. S. Li, J. F. Zhu, P. Liu, F. Yang, G. X. Wang, X. H. Bao, J. Am. Chem. Soc. 2017, **139**, 5652−5655.